*Al Azhar Bulletin of Science Vol. 29, No. 2 (December), 2018, pp. 143-163.*

# MINERALOGY AND RADIOACTIVITY OF THE SOUTHERN PART OF NASSER LAKE SEDIMENTS, EGYPT

**El Azab, A., El Alfi, S.M. and Ali, H. H.**

*Nuclear Materials Authority. P.O. Box 530, El Maadi, Cairo, Egypt.*

## ABSTRACT

*Nasser Lake area delineated by Latitudes 22°00′ –23°58′ N and Longitudes 30°07′–33°15′ E. The identified heavy mineral assemblages of 64 collected representative samples of the study area can be classified into two main groups. The first one is the opaque minerals as; magnetite, hematite, ilmenite, leucoxene, vanadium, chromite, pyrite, atacamite, alumina minerals, gold and silver. The second group is non-opaque minerals includes garnet, monazite, rutile, zircon, titanite, apatite and green silicates (pyroxene and amphibole groups with other minerals such as: epidote, biotite, muscovite, andalusite and sillimanite).*

*The examined sediments of studied area are characterized by radiometrically (low) concentrations of eU and eTh. The radiometrically elemental concentration of eU ranges between U/D and 4ppm with an average of 1.3ppm, while eTh is between 2 and 17ppm with an average of 5.61ppm. The Ra content ranges between 1and 4ppm with an average of 1.66ppm. The content of K ranges between 0.68% and 1.25% with an average of 0.61%.*

## INTRODUCTION

Nasser Lake is located on the border between Egypt and Sudan. It lies between Latitudes 20° 27′ N–23° 58′ N and Longitudes 30° 07′–33° 15′ E. The northern two-third parts of the lake is located in Egypt (always called Nasser Lake), whereas the southern third part is located in Sudan (sometimes called Lake Nubia).

Egypt has constructed a huge human controlled structure "High Aswan Dam" to manage the Nile water and rescue the Nile Delta and flood plain from flooding. At the upstream side of this dam, a huge reservoir was formed, which is called Lake Nasser. The lake stores water budget of Egypt 55.5 BCM per year to secure the water usage in the country (Abul-Atta, 1978). It also receives huge amount of sediments that carried with the water flow from the catchments of the Nile River. The tunnels of the High Aswan Dam allow water to drain downstream into the Nile River, however sediments continuously settle down and accumulate in the lake deforming and reducing the storage capacity.

In the case of full storage capacity, the water level reaches 182 m (A.S.L.) and the lake extends from the Aswan High Dam in Egypt to Dal Cataract in Sudan with length of about 500 km (Fig. 1). At this level, the lake occupies an area of about 6,500 $km^2$ whereas its storage capacity reaches about 162 billion-$m^3$ (Abul-Atta, 1978). This creates a maximum width of about 24 km and a maximum depth of about 110 m.

It is estimated that more than 134 million tons of Nile sediments are deposited annually in Lake Nasser (Shalash, 1980). Depending on this estimation, it could be estimated that there were about 6.8 milliard tons of sediments deposited along the lake since the construction of the dam till 2015. Owing to the strategic importance of the preservation of the lake storage capacity and the priority of sediments as an essential component of the lake system, there is an essential need for understanding the sedimentation processes. Up till now, there is no precise information about the materials beneath the surface of the sediments of Lake Nasser.

Lake Nasser is located in a complex geological area; therefore, it is underlain and surrounded by a wide variety of lithology like granite, gneisses, schists, sandstones, conglomerates and shales. The area is highly affected by structural elements like folds, faults and fractures, which highly controlled the lake path.

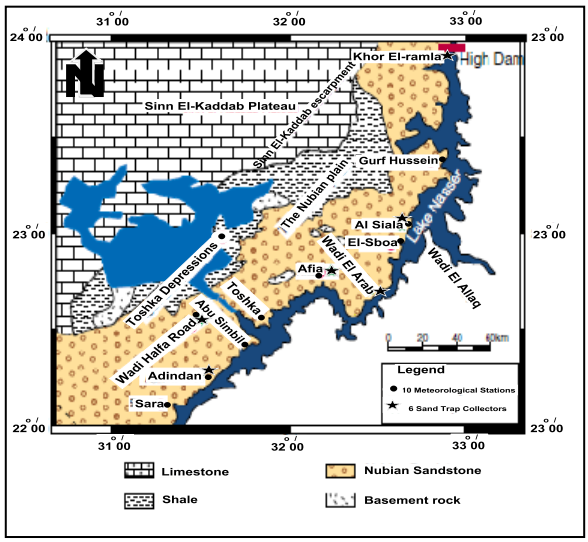


**Figure (1): Litholological map of the study area, after Khedr et al. (2014)**

The lithological variation around the lake body controls the differentiation of the lake into its southern and northern parts around Gomay. The hard basement rocks surrounding the lake along the southern part may be responsible for the narrowing of the lake course. However, the softer sedimentary rocks surrounding the lake along the northern part may be responsible for the widening of the lake course. Therefore, the changes in the hydro-morphologic features (depth, width and hence profile area), to a large extent, appear to be litho-structurally controlled.

Minerology of sand fraction included in the bottom sediments was investigated using the polarized light microscopic technique (Philip et al. 1978). Whereas, the clay mineralogy was investigated using X-ray Florescence Diffraction Technique (XRFD) (El-Kobtan, 2007, El-Kobtan et al., 2016 and Makary, 1982). Said (1981) concluded that, The Nile Delta beaches and nearshore environments have concentration of heavy minerals which originally derived from weathering of the Ethiopian high plateau and transported by Nile River during summer flood seasons to the receiving basin and the southeastern Mediterranean shores. Hassaan and El Dardir (1987) stated that the heavy minerals tend to concentrate in the sand fractions 0.250-0.125mm and 0.125-0.063mm separated from the sediments of the High Dame Lake ranges from 1.5-2% of their total amount. Goher et al. (2014) concluded that eight heavy metals were measured seasonally in the sediments of Nasser Lake during 2013. The abundance of these metals was in the order of Fe> Mn> Zn> Cr> Ni > Cu> Pb>Cd, with mean concentrations of 12.41 mg/g, 279.56, 35.38, 30.79, 27.56, 21.78, 11.21 and 0.183 mg/g, respectively. Khedr et al. (2014) studied and surveyed the three sets of Landsat™ satellite images for the years 1993, 1998&2003 and concluded that, the sand dunes at the south Western Desert of Egypt are generally moving towards southeast direction with a mean annual creeping speed over ground attaining 15 m/year. The total annual estimated volume of transported sand which falls down into Nasser Lake basin attains 16,225,808m3 as calculated by Bagnold's equation and the quantities of sand collected from the sand traps. Farhat and Salem (2015) stated that Lake Nasser sediments are heterogeneous and are mainly silty clay and clayey silt. Eastern and Western sides of the lake include more sand. Gindy (2015) mentioned that the quartz grains in the studied khors sediments of Lake Nasser indicate the presence of mechanical and chemical features and the surface features revealed its history of sedimentation. Such history is reflected by aeolian process, fluvial sedimentation and diagenesis by silica precipitation and dissolution.

The climatic condition is typical arid environment with high temperature that reaches as high as 45°C in June and as low as 5°C in January. It also has nearly no precipitation that classified this region as one of the driest areas in the world. Such conditions have classified this region as hyper-arid (Springuel et al. 1991).

## Geologic setting

The geology of the western shoreline of Lake Nasser area is dominated by a sedimentary succession ranging in age from Jurassic to Quaternary, with exposures of igneous and metamorphic rocks belonging to the Late Precambrian basement, in addition to the Tertiary foreland volcanics of the Late Cretaceous and Mid-Tertiary age (Elewa 2006). Figure 1 shows the geologic map of the study area and the Nubian Sandstone sequence is widely distributed throughout the area. It forms a succession of sandstone beds of different colors with intercalations of clay, siltstone and shale (Fig. 2).

**Figure (2): Photograph shows succession of sandstone beds of different colors with intercalations of clay, siltstone and shale.**

Its thickness increases from the southwest to the north and northwest (El Ramly, 1973). The lower part of the sequence consists of undifferentiated conglomerate, sandstone and shale, while the middle part composed of coarse pebbly sandstone, fine sandstone with siltstone and shale intercalations. The upper part formed of sandstone capped by karstified Tertiary limestone (Kim and Sultan 2002). The Quaternary sediments are represented by conglomerate sheets, sand dunes and sand sheets, where they cover extensive isolated areas in the Nubian plain.

In Lake Nasser area, the structures of the sedimentary succession are directly related to the structures of the basement rocks. The study area is characterized by four different striking major fault systems as follows (El Ramly 1973):

* Wadi El Allaqi strike: this trend possesses NW–SE direction running parallel to the Red Sea graben. Most of the khors in the southern section of Lake Nasser follow this trend.

* Khor Kalabsha-Khor Rahma strike: this trend is E-W and cuts the N-S on the eastern and western sides of the lake as well as the limestone plateau. The extension of this trend ranges between 25 and 130 km.

* Adindan–Tomas and El Sibu–Garf Hussein Strike: have NE–SW trending faults. Extension of these faults reaches a distance ranging between 3 and 60 km.

* Garf Hussein–Aswan strike: it is N-S direction. This extension ranges between 3 and 100 km. The average throw range is between 3 and 60 12m.

## Sampling and techniques

A total of 64 sedimentary samples were collected from the southern part of Nasser Lake. These samples are located on the photo of Google Earth (Fig. 3). The average weight of each sample is about 3kg. The auger is used to collect the samples (Fig. 4a-d).

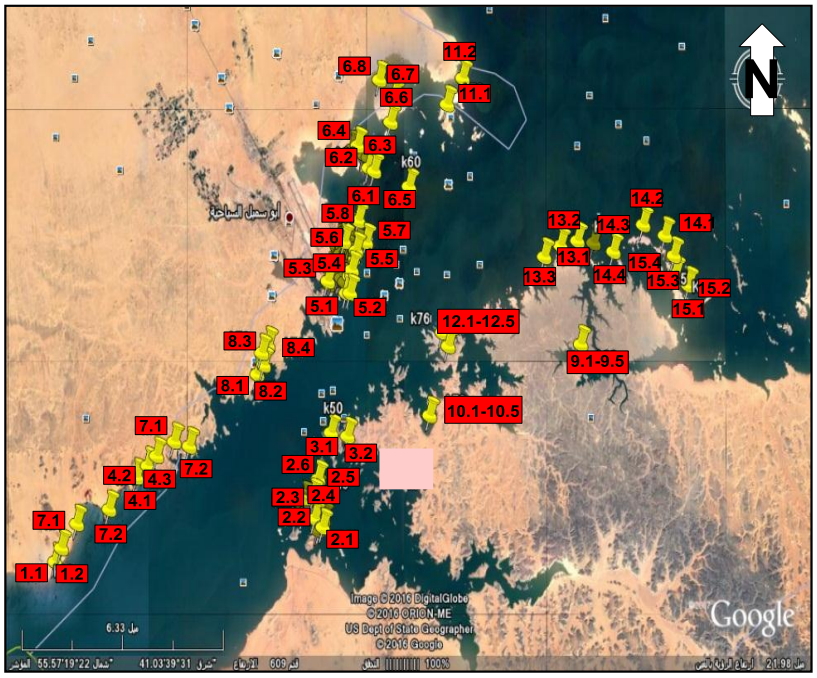


**Figure (3): Photograph of google earth shows distribution of samples locations**

## MINERALOGY

### Preparation of samples and techniques

Muller (1967) stated that, the carbonates and sulphates strongly related to diagenesis. All mineral species with a specific gravity of more than 2.86g/cm$^3$ are traditionally considered as heavy minerals proper. These investigations were done on the sand size less than 0.5mm. Mohamed (1998) stated that the total heavy minerals were concentrated in the medium, fine and very fine sand sizes fraction. The collected 64 representative samples covering the study area are used for further studies.

The original sand sample was dried and prepared for mineral separation by heavy liquid separation using bromoform solution (Sp. Gr. 2.88 g/cm$^3$). Heavy fractions were dried, weighted and their percentages were calculated and tabulated in table 1. The light fractions were discarded, while the heavy fractions are used in further analysis. The magnetite separation carried out using a small hand magnet with suitable strength. The percentages of total heavy bromoform free of magnetite and magnetite were calculated and tabulated in table 2. The heavy minerals assemblage free of magnetite were magnetically fractionated using the laboratory Frantz Isodynamic Magnetic Separator (Model L-1) at side slope of 5°, forward slope of 20° (Flinter,1955).

The identified heavy mineral assemblages studied under a Binocular Stereomicroscope can be classified into two main groups according to Folk (1980). The first one is opaque minerals which includes native minerals as gold and silver; iron oxides as magnetite, hematite, ilmenite and leucoxene, a very low percentage of vanadium, chromite and pyrite; copper minerals as atacamite and alumina minerals. The second group is non-opaque minerals includes silicate minerals as zircon and garnet; phosphate minerals as monazite and apatite; titanium minerals as rutile and titanite; and green silicates (pyroxene and amphibole groups with other minerals such as: epidote, biotite, muscovite, andalusite and sillimanite). The percentage and averages of each mineral is related to the original samples for the studied sediments and tabulated in tables 3 and 4.

Mineralogical investigation of the mineral constituents was carried out by Semi-quantitative EDX and the chemical analyses


**Figure (4): Photographs show shallow water (a&b) and islands (c&d)**

were carried out using a Phillips XL-30 Environmental Scanning Electron Microscope (ESEM) on individual grains of heavy minerals. The most important heavy minerals will be described in the following paragraphs:

**Opaque minerals**
**Native minerals**
**Gold**

Hammoud and Khazback (1984) stated that the percentage of native gold in the black sand samples from El Arish locality (North Sinai) were 1.42g/ton (2204lbs). In different samples from Damietta and Rosetta beach sands, the gold grains were found to range from 0.57 g/ton to 1.7 g/ton. A tentative estimation of gold concentration in the heavy minerals of the Egyptian Northern alluvial-littoeal deposits is about 0.85g/ton.

Hassaan et al. (1995) said that the heavy minerals are found in two grain sizes 0.250-0.125mm and 0.125-0.063mm were chemically analyzed for gold and silver by using the atomic absorption spectrometric methods in the

**Table (1): Percentages of total heavy bromoform (H. Br) for the studied sediments.**

| S. No. | H.Br. % | S. No. | H.Br. % | S. No. | H.Br. % | S. No. | H.Br. % |
|---|---|---|---|---|---|---|---|
| **1.1** | 2.182 | **5.4** | 1.701 | **8.2** | 0.930 | **12.1** | 0.744 |
| **1.2** | 1.170 | **5.5** | 1.239 | **8.3** | 1.044 | **12.2** | 0.575 |
| **2.1** | 1.537 | **5.6** | 1.763 | **8.4** | 0.780 | **12.3** | 0.666 |
| **2.2** | 1.847 | **5.7** | 2.200 | **9.1** | 0.520 | **12.4** | 0.688 |
| **2.3** | 1.977 | **5.8** | 1.107 | **9.2** | 1.262 | **12.5** | 1.039 |
| **2.4** | 1.492 | **6.1** | 15.268 | **9.3** | 0.408 | **13.1** | 0.499 |
| **2.5** | 1.648 | **6.2** | 15.288 | **9.4** | 0.741 | **13.2** | 2.295 |
| **2.6** | 1.528 | **6.3** | 16.933 | **9.5** | 0.981 | **13.3** | 0.499 |
| **3.1** | 1.432 | **6.4** | 16.796 | **10.1** | 0.793 | **14.1** | 0.812 |
| **3.2** | 2.414 | **6.5** | 17.124 | **10.2** | 0.794 | **14.2** | 0.456 |
| **4.1** | 7.872 | **6.6** | 19.976 | **10.3** | 0.569 | **14.3** | 0.535 |
| **4.2** | 8.787 | **6.7** | 17.461 | **10.4** | 0.779 | **14.4** | 0.471 |
| **4.3** | 9.834 | **6.8** | 27.228 | **10.5** | 1.336 | **15.1** | 1.237 |
| **5.1** | 1.384 | **7.1** | 0.730 | **11.1** | 1.816 | **15.2** | 1.368 |
| **5.2** | 1.458 | **7.2** | 0.654 | **11.2** | 1.455 | **15.3** | 1.495 |
| **5.3** | 0.710 | **8.1** | 1.891 | **11.3** | 1.773 | **15.4** | 0.778 |

**Table (2): Percentages of total heavy bromoform free of magnetite and magnetite of Nasser Lack area.**

| S. No. | H.Br.% | Mgt.% | S. No. | H.Br.% | Mgt.% | S. No. | H.Br.% | Mgt.% | S. No. | H.Br.% | Mgt.% |
|---|---|---|---|---|---|---|---|---|---|---|---|
| **1.1** | 2.057 | 0.125 | **5.4** | 1.621 | 0.079 | **8.2** | 0.913 | 0.016 | **12.1** | 0.727 | 0.017 |
| **1.2** | 0.759 | 0.411 | **5.5** | 1.054 | 0.184 | **8.3** | 1.011 | 0.033 | **12.2** | 0.566 | 0.009 |
| **2.1** | 1.440 | 0.097 | **5.6** | 1.590 | 0.173 | **8.4** | 0.767 | 0.014 | **12.3** | 0.656 | 0.010 |
| **2.2** | 1.808 | 0.039 | **5.7** | 2.026 | 0.174 | **9.1** | 0.514 | 0.007 | **12.4** | 0.668 | 0.020 |
| **2.3** | 1.915 | 0.063 | **5.8** | 0.921 | 0.186 | **9.2** | 1.225 | 0.038 | **12.5** | 1.008 | 0.031 |
| **2.4** | 1.423 | 0.069 | **6.1** | 13.394 | 1.874 | **9.3** | 0.400 | 0.008 | **13.1** | 0.488 | 0.011 |
| **2.5** | 1.596 | 0.052 | **6.2** | 13.629 | 1.659 | **9.4** | 0.726 | 0.015 | **13.2** | 2.239 | 0.056 |
| **2.6** | 1.474 | 0.055 | **6.3** | 14.960 | 1.973 | **9.5** | 0.967 | 0.014 | **13.3** | 0.492 | 0.007 |
| **3.1** | 1.191 | 0.242 | **6.4** | 15.932 | 0.864 | **10.1** | 0.764 | 0.029 | **14.1** | 0.801 | 0.011 |
| **3.2** | 2.140 | 0.275 | **6.5** | 16.364 | 0.759 | **10.2** | 0.769 | 0.026 | **14.2** | 0.447 | 0.009 |
| **4.1** | 7.000 | 0.872 | **6.6** | 19.036 | 0.940 | **10.3** | 0.547 | 0.022 | **14.3** | 0.534 | 0.001 |
| **4.2** | 8.075 | 0.712 | **6.7** | 16.733 | 0.728 | **10.4** | 0.761 | 0.018 | **14.4** | 0.464 | 0.007 |
| **4.3** | 9.063 | 0.771 | **6.8** | 25.731 | 1.497 | **10.5** | 1.295 | 0.041 | **15.1** | 1.206 | 0.032 |
| **5.1** | 1.305 | 0.079 | **7.1** | 0.695 | 0.035 | **11.1** | 1.751 | 0.065 | **15.2** | 1.336 | 0.032 |
| **5.2** | 1.281 | 0.177 | **7.2** | 0.630 | 0.024 | **11.2** | 1.408 | 0.047 | **15.3** | 1.454 | 0.040 |
| **5.3** | 0.536 | 0.174 | **8.1** | 1.856 | 0.035 | **11.3** | 1.703 | 0.070 | **15.4** | 0.760 | 0.018 |

**Table (3): The percentage of total heavy opaque minerals of Nasser Lack area.**

| S. No. | Native Elements | | Iron Oxides | | | |
|---|---|---|---|---|---|---|
| | Gold% | Silv.% | Mgt.% | He.% | Ilm.% | Leuco.% |
| **1.1** | 0.016 | 0.004 | 0.125 | 0.029 | 0.678 | 0.087 |
| **1.2** | Nil | Nil | 0.411 | 0.011 | 0.290 | 0.027 |
| **2.1** | 0.018 | 0.006 | 0.097 | 0.037 | 0.434 | 0.053 |
| **2.2** | Nil | Nil | 0.039 | 0.046 | 0.577 | 0.069 |
| **2.3** | Nil | Nil | 0.063 | 0.045 | 0.585 | 0.073 |
| **2.4** | Nil | Nil | 0.069 | 0.064 | 0.428 | 0.067 |
| **2.5** | Nil | Nil | 0.052 | 0.065 | 0.464 | 0.071 |
| **2.6** | Nil | Nil | 0.055 | 0.061 | 0.457 | 0.063 |
| **3.1** | 0.009 | 0.005 | 0.242 | 0.019 | 0.179 | 0.014 |
| **3.2** | Nil | Nil | 0.275 | 0.033 | 0.333 | 0.031 |
| **4.1** | 0.105 | 0.029 | 0.872 | 0.007 | 1.217 | 0.308 |
| **4.2** | Nil | 0.025 | 0.712 | 0.019 | 1.836 | 0.534 |
| **4.3** | Nil | Nil | 0.771 | 0.020 | 1.882 | 0.603 |
| **5.1** | Nil | Nil | 0.079 | 0.051 | 0.026 | 0.281 |
| **5.2** | Nil | Nil | 0.177 | 0.023 | 0.349 | 0.212 |
| **5.3** | Nil | Nil | 0.174 | 0.009 | 0.112 | 0.113 |
| **5.4** | Nil | Nil | 0.079 | 0.019 | 0.266 | 0.506 |
| **5.5** | Nil | Nil | 0.184 | 0.013 | 0.178 | 0.311 |
| **5.6** | Nil | Nil | 0.173 | 0.016 | 0.279 | 0.409 |
| **5.7** | Nil | Nil | 0.174 | 0.024 | 0.368 | 0.453 |
| **5.8** | Nil | Nil | 0.186 | 0.012 | 0.168 | 0.205 |
| **6.1** | 0.107 | 0.058 | 1.874 | 0.078 | 2.070 | 0.323 |
| **6.2** | Nil | Nil | 1.659 | 0.074 | 2.407 | 0.351 |
| **6.3** | Nil | Nil | 1.973 | 0.106 | 1.496 | 0.338 |
| **6.4** | Nil | Nil | 0.864 | 0.136 | 2.566 | 0.459 |
| **6.5** | Nil | Nil | 0.759 | 0.124 | 2.665 | 0.561 |
| **6.6** | Nil | Nil | 0.940 | 0.147 | 3.207 | 0.587 |
| **6.7** | Nil | Nil | 0.728 | 0.169 | 2.755 | 0.455 |
| **6.8** | Nil | Nil | 1.497 | 0.168 | 4.413 | 0.747 |
| **7.1** | 0.007 | 0.001 | 0.035 | 0.009 | 0.202 | 0.138 |
| **7.2** | Nil | Nil | 0.024 | 0.011 | 0.200 | 0.118 |
| **8.1** | 0.022 | 0.004 | 0.035 | 0.241 | 0.373 | 0.654 |
| **8.2** | Nil | Nil | 0.016 | 0.122 | 0.224 | 0.314 |
| **8.3** | Nil | Nil | 0.033 | 0.126 | 0.217 | 0.370 |
| **8.4** | Nil | Nil | 0.014 | 0.099 | 0.161 | 0.271 |
| **9.1** | 0.005 | 0.002 | 0.007 | 0.060 | 0.119 | 0.112 |
| **9.2** | Nil | Nil | 0.038 | 0.149 | 0.284 | 0.269 |
| **9.3** | Nil | Nil | 0.008 | 0.048 | 0.092 | 0.088 |
| **9.4** | Nil | Nil | 0.015 | 0.082 | 0.171 | 0.162 |
| **9.5** | Nil | Nil | 0.014 | 0.107 | 0.214 | 0.216 |
| **10.1** | 0.005 | 0.001 | 0.029 | 0.010 | 0.272 | 0.181 |
| **10.2** | Nil | Nil | 0.026 | 0.012 | 0.258 | 0.181 |
| **10.3** | Nil | Nil | 0.022 | 0.008 | 0.187 | 0.127 |
| **10.4** | Nil | Nil | 0.018 | 0.009 | 0.259 | 0.178 |
| **10.5** | Nil | Nil | 0.041 | 0.016 | 0.432 | 0.302 |
| **11.1** | 0.013 | 0.007 | 0.065 | 0.017 | 0.306 | 0.512 |
| **11.2** | Nil | Nil | 0.047 | 0.015 | 0.257 | 0.419 |
| **11.3** | Nil | Nil | 0.070 | 0.016 | 0.309 | 0.513 |
| **12.1** | 0.007 | 0.002 | 0.017 | 0.038 | 0.118 | 0.233 |
| **12.2** | Nil | Nil | 0.009 | 0.028 | 0.087 | 0.179 |
| **12.3** | Nil | Nil | 0.010 | 0.029 | 0.101 | 0.210 |
| **12.4** | Nil | Nil | 0.020 | 0.025 | 0.101 | 0.218 |
| **12.5** | Nil | Nil | 0.031 | 0.015 | 0.164 | 0.331 |
| **13.1** | 0.003 | 0.001 | 0.011 | 0.008 | 0.081 | 0.270 |
| **13.2** | Nil | Nil | 0.056 | 0.035 | 0.369 | 1.247 |
| **13.3** | Nil | Nil | 0.007 | 0.008 | 0.083 | 0.272 |
| **14.1** | 0.007 | 0.001 | 0.011 | 0.012 | 0.135 | 0.404 |
| **14.2** | Nil | Nil | 0.009 | 0.005 | 0.070 | 0.247 |
| **14.3** | Nil | Nil | 0.001 | 0.006 | 0.084 | 0.294 |
| **14.4** | Nil | Nil | 0.007 | 0.006 | 0.072 | 0.250 |
| **15.1** | 0.012 | 0.007 | 0.032 | 0.012 | 0.188 | 0.664 |
| **15.2** | Nil | Nil | 0.032 | 0.013 | 0.205 | 0.749 |
| **15.3** | Nil | Nil | 0.040 | 0.016 | 0.227 | 0.810 |
| **15.4** | Nil | Nil | 0.018 | 0.008 | 0.121 | 0.418 |
| **Min.** | Nil | Nil | 0.001 | 0.005 | 0.026 | 0.014 |
| **Max.** | 0.107 | 0.058 | 1.973 | 0.241 | 4.413 | 1.247 |
| **Aveg.** | 0.008 | 0.004 | 0.253 | 0.048 | 0.616 | 0.316 |

**S. No.**=Sample number, **Gold**=Gold, **Silv.=**Silver, **Mgt.**=Magnetite, **He.**=Hematite**, Ilm.**=Ilmenite, **Leuc.**=leucoxene.

**Table (4): The percentage of total heavy non-opaque minerals of Nasser Lack area.**

| S. No. | Silicate Minerals | | Phosphate Minerals | | Titanium Minerals | | Green Silicate |
|---|---|---|---|---|---|---|---|
| | Zr.% | Gar.% | Mon.% | Apat.% | Rut.% | Tit.% | G. S.% |
| **1.1** | 0.238 | 0.039 | 0.009 | 0.013 | 0.078 | 0.015 | 0.851 |
| **1.2** | 0.135 | 0.014 | 0.002 | 0.005 | 0.020 | 0.005 | 0.250 |
| **2.1** | 0.144 | 0.022 | 0.006 | 0.015 | 0.029 | 0.014 | 0.662 |
| **2.2** | 0.188 | 0.026 | 0.008 | 0.017 | 0.043 | 0.017 | 0.816 |
| **2.3** | 0.197 | 0.028 | 0.007 | 0.018 | 0.043 | 0.018 | 0.900 |
| **2.4** | 0.156 | 0.024 | 0.009 | 0.014 | 0.041 | 0.016 | 0.605 |
| **2.5** | 0.173 | 0.027 | 0.008 | 0.017 | 0.039 | 0.017 | 0.716 |
| **2.6** | 0.157 | 0.017 | 0.005 | 0.011 | 0.037 | 0.014 | 0.652 |
| **3.1** | 0.031 | 0.009 | 0.002 | 0.004 | 0.015 | 0.006 | 0.898 |
| **3.2** | 0.072 | 0.019 | 0.004 | 0.010 | 0.030 | 0.014 | 1.593 |
| **4.1** | 1.429 | 0.060 | 0.021 | 0.130 | 1.603 | 0.058 | 2.033 |
| **4.2** | 0.807 | 0.173 | 0.025 | 0.038 | 1.348 | 0.059 | 3.212 |
| **4.3** | 1.558 | 0.088 | 0.020 | 0.033 | 1.920 | 0.114 | 2.826 |
| **5.1** | 0.067 | 0.019 | 0.005 | 0.005 | 0.188 | 0.015 | 0.648 |
| **5.2** | 0.250 | 0.016 | 0.004 | 0.004 | 0.225 | 0.010 | 0.187 |
| **5.3** | 0.058 | 0.005 | 0.001 | 0.001 | 0.153 | 0.003 | 0.079 |
| **5.4** | 0.242 | 0.033 | 0.001 | 0.004 | 0.213 | 0.021 | 0.316 |
| **5.5** | 0.173 | 0.015 | 0.002 | 0.003 | 0.138 | 0.010 | 0.212 |
| **5.6** | 0.270 | 0.028 | 0.003 | 0.005 | 0.225 | 0.017 | 0.337 |
| **5.7** | 0.374 | 0.028 | 0.004 | 0.006 | 0.314 | 0.018 | 0.436 |
| **5.8** | 0.170 | 0.010 | 0.002 | 0.003 | 0.141 | 0.009 | 0.201 |
| **6.1** | 3.018 | 0.103 | 0.019 | 0.076 | 1.912 | 0.215 | 5.413 |
| **6.2** | 2.713 | 0.106 | 0.018 | 0.101 | 1.728 | 0.355 | 5.775 |
| **6.3** | 4.151 | 0.226 | 0.021 | 0.103 | 2.199 | 0.327 | 5.995 |
| **6.4** | 2.128 | 0.207 | 0.044 | 0.137 | 1.267 | 0.406 | 8.581 |
| **6.5** | 2.067 | 0.188 | 0.030 | 0.150 | 1.221 | 0.508 | 8.850 |
| **6.6** | 1.980 | 0.266 | 0.089 | 0.179 | 1.352 | 0.581 | 10.648 |
| **6.7** | 1.985 | 0.245 | 0.059 | 0.158 | 1.409 | 0.422 | 9.075 |
| **6.8** | 3.019 | 0.310 | 0.046 | 0.262 | 2.106 | 0.611 | 14.049 |
| **7.1** | 0.098 | 0.008 | 0.002 | 0.011 | 0.124 | 0.010 | 0.084 |
| **7.2** | 0.086 | 0.011 | 0.002 | 0.010 | 0.113 | 0.014 | 0.067 |
| **8.1** | 0.163 | 0.022 | 0.006 | 0.019 | 0.205 | 0.024 | 0.123 |
| **8.2** | 0.074 | 0.009 | 0.003 | 0.006 | 0.092 | 0.010 | 0.059 |
| **8.3** | 0.088 | 0.012 | 0.004 | 0.010 | 0.109 | 0.012 | 0.064 |
| **8.4** | 0.074 | 0.008 | 0.002 | 0.007 | 0.088 | 0.008 | 0.049 |
| **9.1** | 0.066 | 0.004 | 0.002 | 0.006 | 0.104 | 0.005 | 0.029 |
| **9.2** | 0.168 | 0.012 | 0.004 | 0.015 | 0.244 | 0.011 | 0.069 |
| **9.3** | 0.056 | 0.004 | 0.001 | 0.005 | 0.080 | 0.003 | 0.023 |
| **9.4** | 0.100 | 0.007 | 0.002 | 0.008 | 0.145 | 0.004 | 0.044 |
| **9.5** | 0.141 | 0.008 | 0.002 | 0.013 | 0.197 | 0.008 | 0.061 |
| **10.1** | 0.083 | 0.016 | 0.001 | 0.009 | 0.162 | 0.002 | 0.020 |
| **10.2** | 0.093 | 0.015 | 0.002 | 0.009 | 0.161 | 0.004 | 0.034 |
| **10.3** | 0.067 | 0.011 | 0.001 | 0.006 | 0.112 | 0.003 | 0.027 |
| **10.4** | 0.089 | 0.016 | 0.002 | 0.011 | 0.153 | 0.005 | 0.039 |
| **10.5** | 0.157 | 0.026 | 0.004 | 0.015 | 0.264 | 0.010 | 0.070 |
| **11.1** | 0.228 | 0.036 | 0.005 | 0.019 | 0.436 | 0.013 | 0.160 |
| **11.2** | 0.184 | 0.026 | 0.004 | 0.013 | 0.346 | 0.012 | 0.131 |
| **11.3** | 0.213 | 0.034 | 0.006 | 0.013 | 0.418 | 0.015 | 0.166 |
| **12.1** | 0.096 | 0.008 | 0.002 | 0.004 | 0.156 | 0.005 | 0.057 |
| **12.2** | 0.076 | 0.007 | 0.001 | 0.003 | 0.136 | 0.003 | 0.045 |
| **12.3** | 0.085 | 0.010 | 0.002 | 0.004 | 0.159 | 0.004 | 0.052 |
| **12.4** | 0.084 | 0.009 | 0.002 | 0.004 | 0.166 | 0.005 | 0.054 |
| **12.5** | 0.132 | 0.015 | 0.002 | 0.006 | 0.254 | 0.008 | 0.082 |
| **13.1** | 0.050 | 0.013 | 0.002 | 0.005 | 0.042 | 0.005 | 0.008 |
| **13.2** | 0.234 | 0.055 | 0.006 | 0.016 | 0.191 | 0.019 | 0.068 |
| **13.3** | 0.050 | 0.012 | 0.001 | 0.003 | 0.042 | 0.004 | 0.016 |
| **14.1** | 0.084 | 0.021 | 0.003 | 0.006 | 0.093 | 0.007 | 0.027 |
| **14.2** | 0.047 | 0.008 | 0.001 | 0.002 | 0.053 | 0.002 | 0.011 |
| **14.3** | 0.055 | 0.010 | 0.001 | 0.004 | 0.064 | 0.003 | 0.014 |
| **14.4** | 0.050 | 0.007 | 0.002 | 0.003 | 0.058 | 0.003 | 0.012 |
| **15.1** | 0.119 | 0.019 | 0.003 | 0.009 | 0.134 | 0.010 | 0.028 |
| **15.2** | 0.139 | 0.021 | 0.004 | 0.008 | 0.151 | 0.012 | 0.034 |
| **15.3** | 0.145 | 0.025 | 0.004 | 0.011 | 0.169 | 0.014 | 0.035 |
| **15.4** | 0.077 | 0.013 | 0.003 | 0.005 | 0.090 | 0.006 | 0.021 |
| **Min.** | 0.031 | 0.004 | 0.001 | 0.001 | 0.015 | 0.002 | 0.008 |
| **Max.** | 4.151 | 0.310 | 0.089 | 0.262 | 2.199 | 0.611 | 14.049 |
| **Aveg.** | 0.495 | 0.045 | 0.009 | 0.028 | 0.399 | 0.065 | 1.386 |

**S. No.**=Sample number **Zr.**=Zircon, **Gar.**=Garnet, **Mon.**=Monazite, **Apat.**= Apatite**, Rut.**=Rutile, **Tit.**=Titanite, **G.S.**=Green Silicates**.**

Central Labs of Geol. Surv. of Egypt. They showed that the gold and silver are restricted to the grain size of 0.125mm between Latitudes 22° 00\ 00\\ to 22° 30\ 00\\ and named this part north sedimentation area (NMSA). Gold content reaches up to 16.36 g/t in this part while reach up to 0.91 g/t in the same grain size in Rosetta.

In our study, the shape of these grains is irregular, wire-like (Fig. 5a) and oval rounded to sub-rounded. Gold grains are clean, uncoated, not tarnish and exhibit golden yellow color particles with brilliant metallic luster. Pure gold grains were investigated under the Environmental Scanning Electronic Microscope (ESEM) and the elemental chemical compositions are shown in figures 5 b, c and d.

Chemically, the analyses of gold using the atomic absorption spectrometric methods in the Central Labs of Geol. Surv. of Egypt are listed in table 5. Gold content ranging from 0.3 gm/ton to 4.54 gm/ton.

**Silver**

Silver has an attractive shiny appearance, although it tarnishes easily. The tarnish is silver sulphide ($Ag_2S$). It is represented by discoidal (platy) grain (Fig. 6a). Pure silver grains were investigated under the Environmental Scanning Electronic Microscope (ESEM) and the elemental chemical compositions are shown in figure 6b. Chemically, the analyses of silver by using the atomic absorption spectrometric methods in the Central Labs of Geol. Surv. of Egypt are tabulated in table 5. Silver content ranging from 0.03 gm/ton to 1.2 gm/ton.

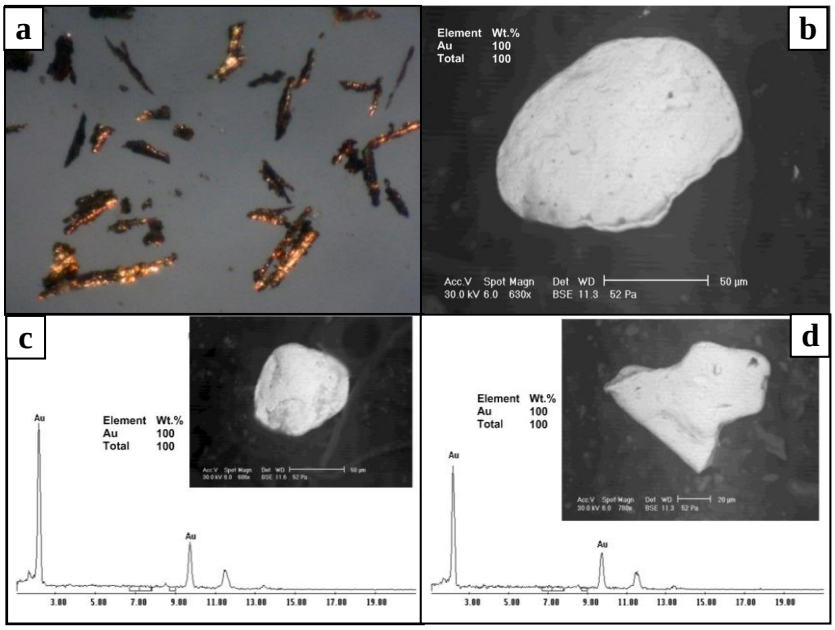


**Figure (5): Photomicrographs show gold grains under binocular stereomicroscope (a), X35, BSE image (b) and EDX analyses of gold grains (c&d).**

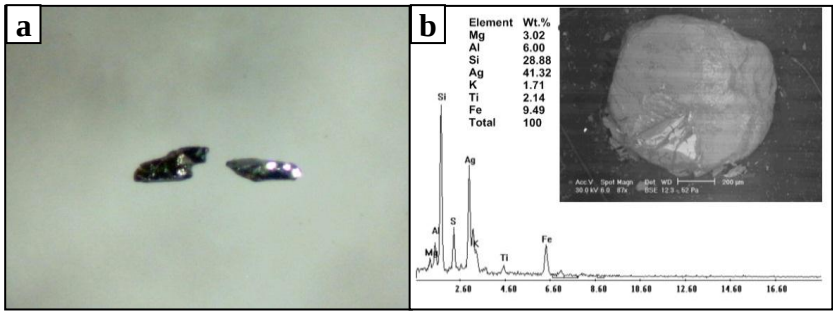


**Figure (6): Photomicrographs show silver grains under binocular stereomicroscope (a), X35, EDX and BSE image of silver grain (b).**

**Table (5): Chemical analyses for gold and silver of the studied samples**

| S.No. | Au. Gm/ton | Ag. Gm/ton | S. No. | Au. Gm/ton | Ag. Gm/ton |
|---|---|---|---|---|---|
| **2.1** | 0.3 | 1.2 | **6.5** | 0.8 | --- |
| **2.3** | 4.54 | --- | **8.1** | 1 | 0.3 |
| **2.5** | 1.24 | --- | **8.3** | 1.24 | --- |
| **2.7** | 3 | --- | **9.1** | 0.5 | 0.1 |
| **4.1** | 1.2 | --- | **9.2** | 0.6 | --- |
| **4.2** | 1.2 | --- | **9.3** | 1 | 0.03 |
| **5.1** | 0.3 | --- | **13.1** | 1.5 | --- |
| **5.2** | 0.8 | --- | **11** | 1 | --- |
| **5.3** | 0.7 | --- | **12** | 3.76 | --- |
| **5.7** | 0.5 | 0.3 | **13** | 2 | --- |
| **6.1** | 2.94 | --- | **14** | 1 | --- |
| **6.2** | 2 | 0.2 | **15** | 0.9 | --- |

## Iron oxides

### Magnetite $Fe_3O_4$

Magnetite displays black to deep reddish brown color, with metallic to dull luster. Their habit ranges from massive, granular, angular to sub-angular and the octahedron crystals of magnetite are less frequent and occur as isolated grains (Fig. 7a) or composite grains with quartz (Fig. 7b). Pure magnetite grains were investigated under the Environmental Scanning Electronic Microscope (ESEM) and the elemental chemical compositions are shown in figure 7c. Due to the preferred incorporation of the elements Mg, Mn, Zn, Ni, Cr, Ti, Al, V in the magnetite lattice, naturally occurring magnetite nearly always has varying percentages of these elements. Magnetite is an important mineral in the mixing triangle FeO-$Fe_2O_3$-$TiO_2$. This explains why magnetite frequently occurs in magmatic and metamorphic rocks in conjunction with ulvite ($Fe_2TiO_4$) and titanomagnetite (solid solution between magnetite and ulvite) as well as ilmenite ($FeTiO_3$) and goethite. These minerals occur either separately from each other or in homogenous fixed compounds or as inclusions within each other (MÜCKE 2003). Titanomagnetite contains up to 13 % $TiO_2$ (Ward &Towner 1985) in the present study the EDX of magnetite (semi quantitative chemical analysis) shows additional weight percent of titanium element reaches up to 22.95%. It was recorded in the all studied sediments as common accessory mineral and its content range from 0.001% to 1.973% with an average of about 0.253%.

### Hematite $Fe_2O_3$

Hematite is the principle ore of iron which originated mainly from magnetite alteration processes and alteration product of many Fe-bearing minerals especially pyrite and so called hematite after pyrite (goethite) or pseudomorphic pyrite (Fig. 8a). The non-crystalline forms of hematite are supposedly transformations of the mineral limonite and occurs as a reddish brown to black color (Fig. 8b), as elongated road like shape with red color (Fig. 8c) angular to sub-angular with metallic or dull in earthy.

Pure hematite grains were investigated under the Environmental Scanning Electronic Microscope (ESEM) and the elemental chemical compositions are shown in figure 8d. It was recorded in all studied sediments as common accessory mineral and its content range from 0.005% to 0.241% with an average of about 0.048%.

### Ilmenite $FeTiO_3$

Ilmenite is a common accessory mineral and considered as a most important ore of titanium. Consequently, it is used as a raw material for pigment production. Ilmenite was recorded as iron-black color with metallic luster. It occurs as angular to subangular grains with sharp edges (Fig. 9a), nearly rounded (Fig.


**Figure (7): Photomicrographs show aggregates of magnetite and composite grains of magnetite and quartz (a&b), X35, EDX and BSE image of titanomagnetite grain (c).**

9b), tabulated thick tabular grains and shows strong striations (Fig. 9c). It is more abundant in the finer sand size than that of the medium sand size. Ilmenite is a ferromagnetic mineral separated mainly at the magnetic fields 0.2A and 0.5A using the Frantz Isodynamic Magnetic Separator. The significance of ilmenite as the most important, rock-forming titanium mineral is not due to the extraction of titanium metal but the production of titanium dioxide ($TiO_2$). Titanium dioxide is easily the most significant white pigment in the world and is used, amongst other things, in paints, printing inks, plastics, rubber, artificial fibers, paper, glass and ceramics (Elsner, 2010). Pure ilmenite grains were investigated under the Environmental Scanning Electronic Microscope (ESEM) and the elemental chemical compositions are shown in figure 9d. It was recorded in the all studied sediments as common accessory mineral and its content ranges from 0.026% to 4.413% with an average of about 0.616%.

**Chromite $FeCr_2O_4$**

Chromite is the main ore of chromium and has a wide range in industrial uses. It is used as a refractory material due to its high heat

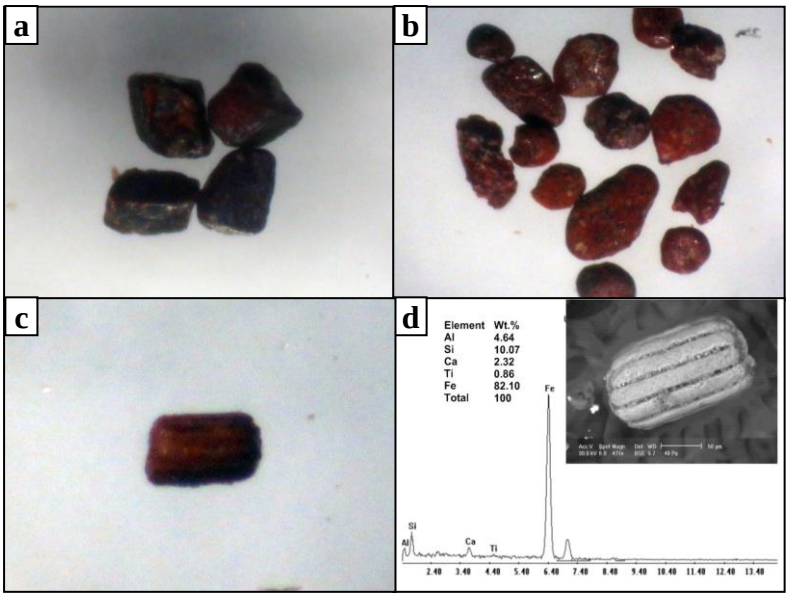


**Figure (8): Photomicrographs show hematite after pyrite (goethite) (a), X35, reddish brown to black color (b), X35, elongated road like shape with red color (c), X70, EDX and BSE image of hematite grain (d).**

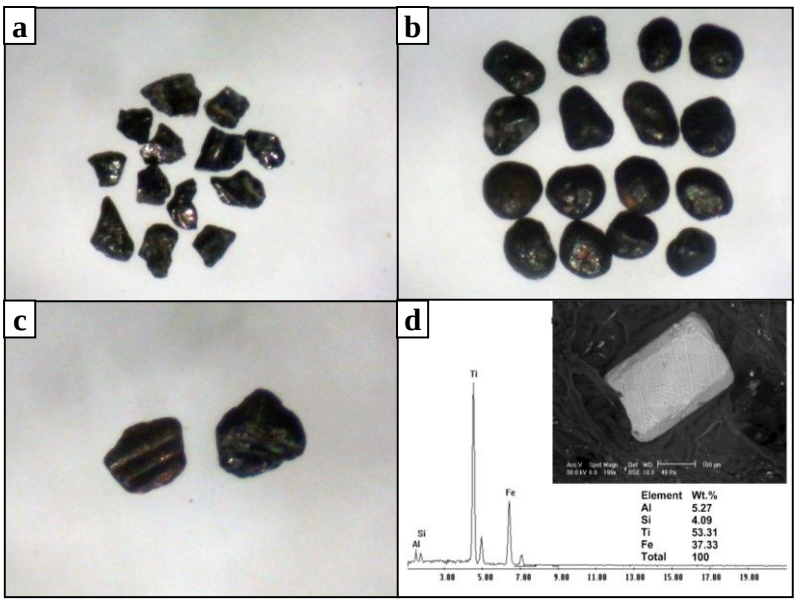


**Figure (9): Photomicrographs show angular to subangular ilmenite grains with sharp edges (a), X35, rounded ilmenite grains (b), X35, strong striations (c), X45, EDX and BSE image of ilmenite grain (d).**

stability. Chromite usually occurs as well formed octahedron crystals. It was separated at 0.2A and 0.5A using Frantz Isodynamic Separator. Its color varies from black to brownish black with metallic luster (Fig. 10a). The EDX/BSE image of chromite octahedron crystals and the elemental chemical compositions are shown in figure 10b.

**Leucoxene (mixture of Fe-Ti oxides)**

Leucoxene is not a mineral but it represents the transitional phase during the alteration of ilmenite to form the secondary rutile (Mohamed, 1987, Mohamed, 1998 and Elsner, 2010). It displays rounded and subrounded habits and smooth or pitted surface. It has yellow to yellowish brown and dark brown color under binocular stereomicroscope and its shape ranges from rounded platy grains to prismatic grains with yellow color (Figs. 11a & 11b). It appears as amorphous materials. Ilmenite occurs as relicts on the surface of leucoxene as indications of alteration processes. Leucoxene was separated at 0.5A and 1.0A, using Frantz Isodynamic Separator but the majority of leucoxene are separated at 1.0A. It was recorded in the all studied sediments as common accessory mineral and its content ranges from 0.014% to 1.247% with an average of about 0.316%.

**Pyrite $FeS_2$**

It is a common sulphide mineral together with chalcopyrite. It has well developed cubic shape with angular faces and subhedral grains with sharp edges. It exhibits golden yellow or shiny brassy yellow color with metallic luster (Fig. 12a). Pyrite was separated at magnetic field strength 1.5A using the Frantz Isodynamic Separator. Pure pyrite grains were investigated under the Environmental Scanning Electronic Microscope (ESEM) as shown in figure 12b with its EDX and the elemental chemical compositions shows the pure composition.

**Vanadium Minerals**
**Native vanadium**

Vanadium is an essential trace element for most species. Vanadium is a soft, shiny, bright silvery-white metal and irregular to flattened grains (Fig. 13a**).** It exhibits corrosion-resistant, except to most acids. Vanadium grains were investigated under the Environmental Scanning Electronic Microscope (ESEM) and the elemental chemical compositions clears inclusion from S, Pb, Na, Cr and Fe elements as shown in figures 13b, c and d. Vanadium is used in ceramics, glass and dyes as well as a chemical catalyst.

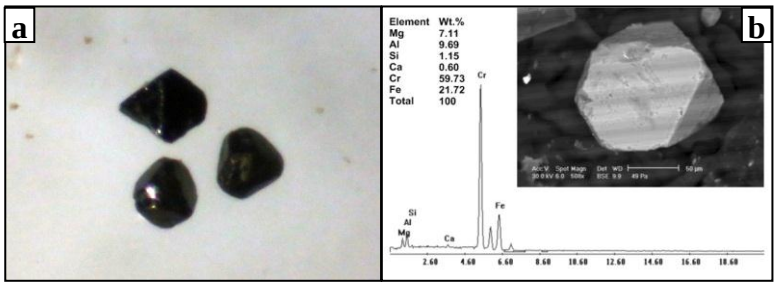


**Figure (10): Photomicrographs show black chromite (a), X60, EDX and BSE image of octahedron chromite grain (b).**

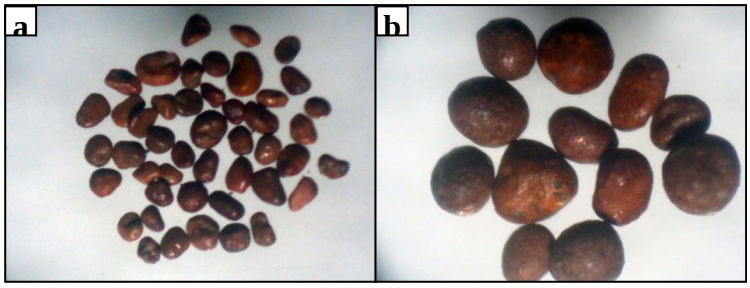


**Figure (11): Photomicrographs show normal sizes of leucoxene grains (a), X20 and large sizes of leucoxene grains (b), X20.**

**Copper Minerals**
**Atacamite $Cu_2Cl(OH)_3$**

Atacamite was recorded in some samples of the studied area by very rare trace non-magnetic minerals. It is a comparatively rare mineral, formed from primary copper minerals in the oxidation conditions. It has green color (Fig. 14a) with dull luster (Phillips and Griffen 1981). Their crystals are transparent to translucent. The grains here are translucent. Pure atacamite grains were investigated under the Environmental Scanning Electronic Microscope (ESEM) and the elemental chemical compositions are shown in figure 14b.

**Alumina minerals**

Aluminum is a relatively soft, nonmagnetic, ductile and malleable silvery metal. It is the most common metal present in the Earth's crust and the third most common element (after oxygen and silicon). It is moderately reactive and never found in pure form in nature. It exhibits grayish-white color, metallic luster and massive grains with platy or scaly aggregates (Figs.15a&b). Pure aluminum grains were investigated under the Environmental Scanning Electronic Microscope (ESEM) and the elemental chemical compositions are shown in figures 15c and d. Aluminum has hundreds of uses, from aircraft and vehicle parts to building material, beverage cans, wrapping foil and just about any applications where a lightweight metal is needed.

**Non-Opaque Minerals**
**Silicate Minerals**

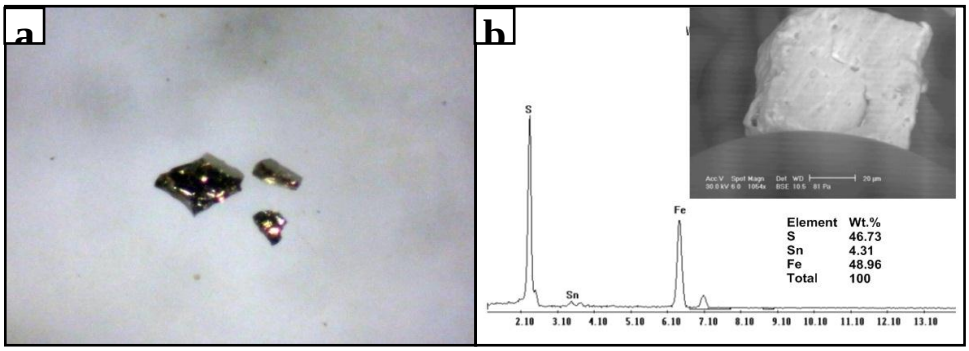


**Figure (12): Photomicrographs show pyrite grains (a), X35, EDX and BSE image of pyrite grain (b).**

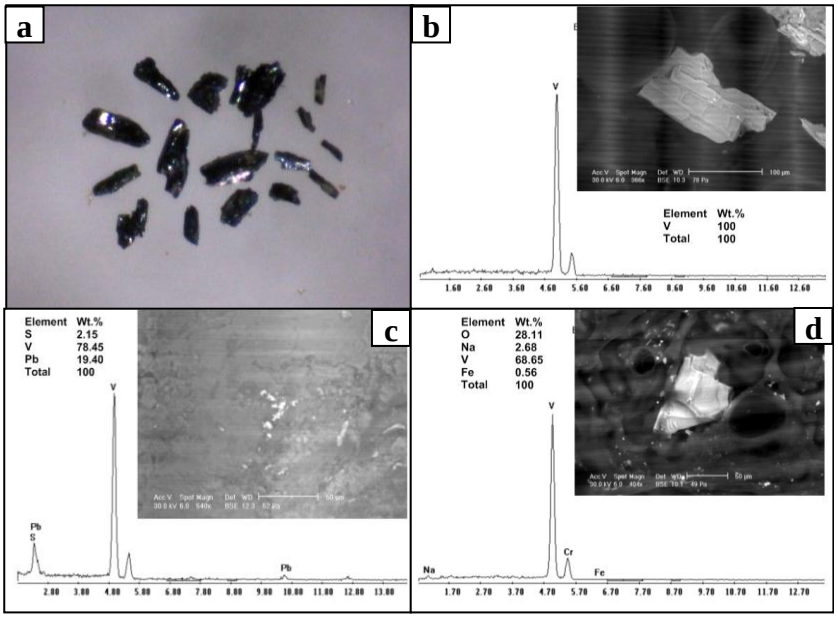


**Figure (13): Photomicrographs show vanadium grains (a), X35, EDX and BSE image of Native vanadium grain, (b). EDX and BSE image of different elements inclusion in vanadium grain (c&d).**

**Zircon $ZrSiO_4$**

Most of zircon grains have an euhedral external morphology. It was recorded as short to long prismatic with pyramid termination; also some grains were recorded as sub-rounded to rounded. However, it is concentrated in both nonmagnetic and magnetic fractions at 1.5A. Zircon separated in the nonmagnetic field 1.5A has long prismatic water clear color with vitreous luster (Fig. 16a). Armstrong (1922), Groves (1930), Poldervart (1955-1956) and Saxena (1966) stated that the water clear zircon grains in all types of rocks are nonmagnetic.

On the other hand, the magnetic zircon grains are short prismatic, black to blackish brown, reddish yellow and yellow (Fig. 16b) with vitreous luster. The variation in the color of zircon may be attributed to the density of fine inclusions as well as the degree of iron oxides staining. Some inclusions may be due to iron ions that could penetrate from the original melt through zircon lattice during magmatic crystallization or from an outside source (Hassan 2005 and Surour et al., 2003). These inclusions are considered as weak points which accelerate the disintegration of the grains (Carrol, 1953). Pure zircon grains were investigated under the Environmental Scanning Electronic Microscope (ESEM) and the elemental chemical compositions are shown in figure. 16c.

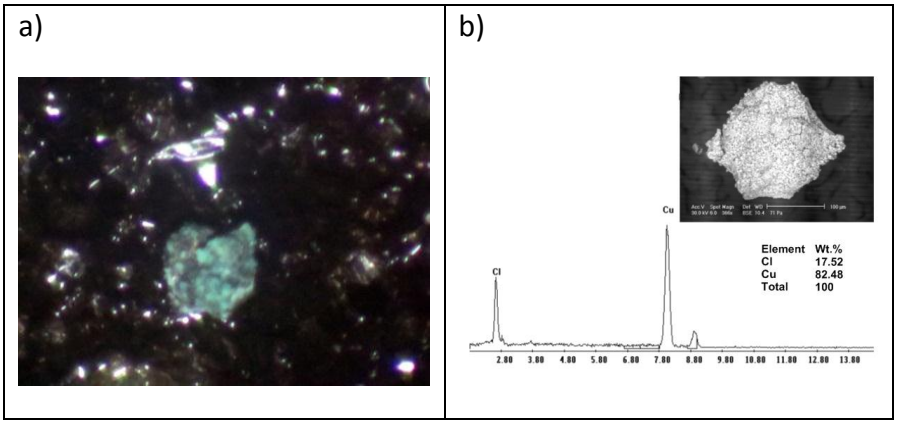


**Figure (14): Photomicrographs show green color atacamite grain (a), X45, EDX and BSE image of atacamite grain (b).**

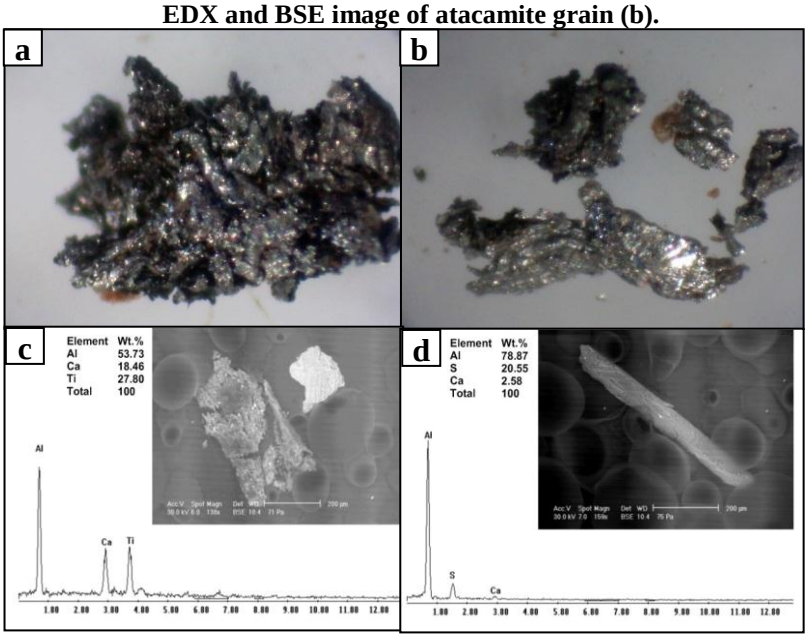


**Figure (15): Photomicrographs show:**

**a) Grayish-white color and metallic luster of aluminum grains, X35.**

**b) Platy or scaly of aluminum grains, X35. c and d) EDX and BSE image of alumina grain.**


**Figure (16): Photomicrographs show:**
**a) Colorless zircon grains, X35.**
**b) Black to blackish brown, reddish yellow and yellow zircon grains, X35.**
**c) EDX and BSE image of pure zircon grain.**

**Garnet**

Garnet is a group of minerals closely related in physical and chemical properties. The minerals of garnet group characterize some metamorphic rocks, others occur in high-pressure igneous rocks. It was recorded in the studied samples as euhedral to anhedral colorless almandine grains with sharp edges (Fig. 17a), deep rose almandine-spessartine solid solution (Fig. 17b) and green tsavorite (Fig.17c). Garnet was separated at magnetic field strength 0.2A and 0.5A using the Frantz Isodynamic Separator. Pure garnet grains were investigated under the Environmental Scanning Electronic Microscope (ESEM) and the elemental chemical compositions as shown in figures 17d, e and f.

**Phosphate Minerals**
**Monazite [$CeLaPO_4$]**

It is a rare earth phosphate of highly variable composition. It exhibits high content from thorium and uranium; therefore, it is documented as radioactive mineral. Monazite exhibits shape varies from rounded to oval. Its color ranges from colorless (Fig. 18a), honey to lemon yellow (Fig.18b). It occurs as accessory mineral in fine and very fine sand size fractions in the studied samples. It was separated at magnetic field strength 0.5A and 1.0A using the Frantz Isodynamic Separator. The EDX/BSE image of monazite and the elemental chemical compositions are shown in figure 18c.

**Apatite $Ca_5 (PO_4)_3F$**

Apatite is one of few minerals that are produced and used by biological micro-environmental systems. It is the most common phosphate mineral and is the main source of the phosphorus required by plants. The bones and teeth of most animals, including humans, are of the same material. It was recorded in all studied samples. Its color ranges from colorless (Fig. 19a) to yellow (Fig. 19b). The EDX/BSE image of apatite and the elemental chemical compositions show prismatic colorless apatite (Fig. 19c) and oval yellow apatite (Fig. 19d).

**Titanium Minerals**

**Rutile $TiO_2$**

It is considered as a major ore of titanium. Rutile occurs as euhedral and anhedral grains, rounded (Figs. 20a & b), prismatic (Figs. 20c & d), elongated tabular or needle-like crystals. The prismatic grains as well as the chevron (elbow) rutile variety are very common. The elbow rutile twins (Fig. 20e) produce in the crystalline form at a near 60 degree angle. Rutile crystallized in tetragonal system in the form of ditetragonal dipyramidal (Fig. 20f). Rutile varies in color from red (Figs 20a, c & e) to blood red to opaque (Fig. 20b, d & f). The majority of rutile grains were separated at magnetic field strength of 1.5A and the rest of rutile were founded in nonmagnetic 1.5A fraction using the Frantz Isodynamic Separator. The opaque variety is frequent in the highly magnetic, while yellowish and reddish (translucent) rutile increases in the nonmagnetic fraction. Pure rutile grains were investigated under the Environmental Scanning Electronic Microscope (ESEM) and the elemental chemical compositions are shown in figures 20g & h.

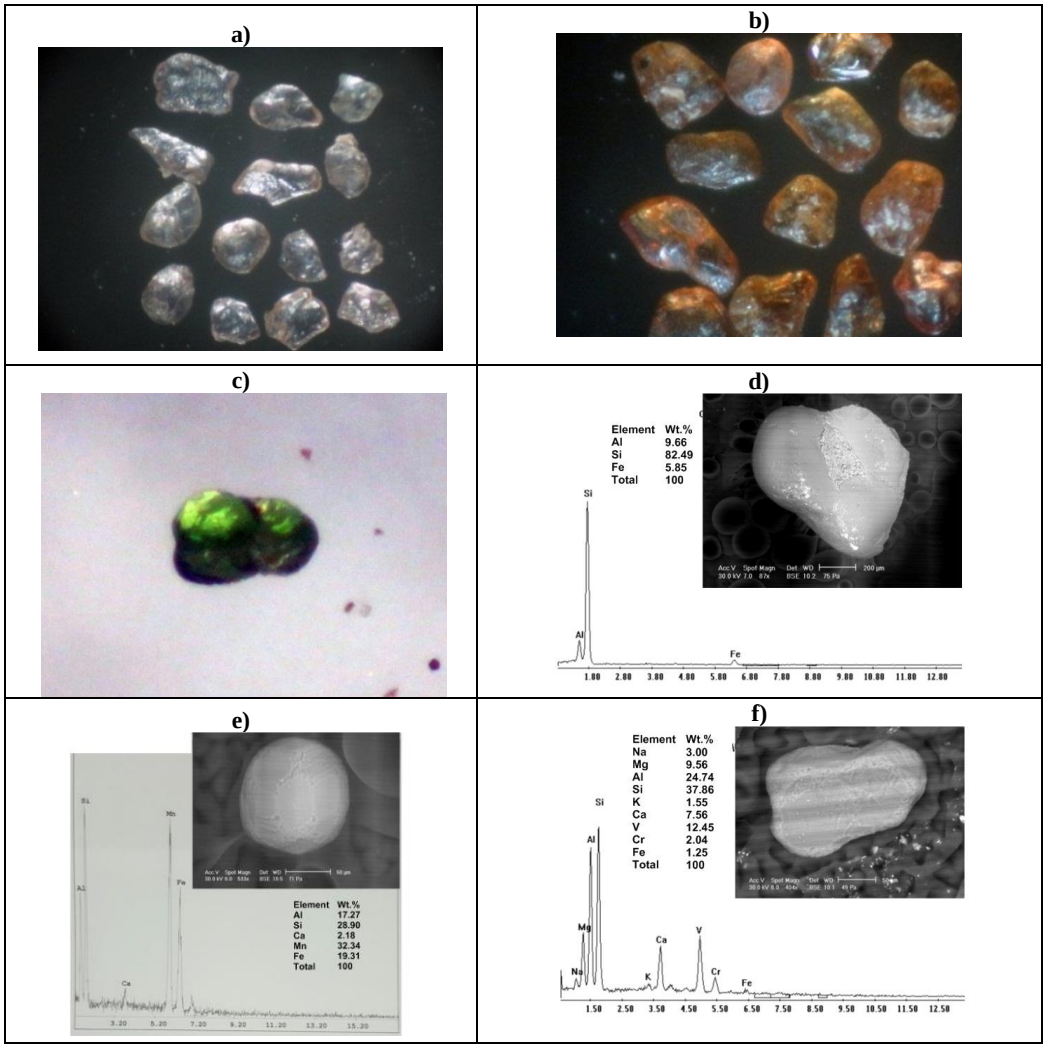


**Figure (17): Photomicrographs show:**
**a) Almandine garnet grains, X25. b) Almandine-spessartine solid solution, X35.**
**c) Tsavorite, X35. d) EDX and BSE image of colorless almandine garnet grain.**
**e) EDX and BSE image of deep rose almandine-spessartine garnet grain.**
**f) EDX and BSE image of green tsavorite garnet grain.**

### Titanite (Sphene) Ca Ti Si $O_5$

Titanite is more common in all samples of the studied area. Its color varies from yellowish to brownish yellow with vitreous luster. Titanite mineral grains are subhedral to anhedral of adamantine luster with imperfect cleavage (Fig. 21a). Titanite was separated at magnetic field strength 1.0A and less common in 0.5A using the Frantz Isodynamic Separator. Pure titanite grains were investigated under the Environmental Scanning Electronic Microscope (ESEM) and the elemental chemical compositions as shown in figure 21b.

### Thorite [$ThSiO_4$]

Thorite occurs in nature as a primary mineral chiefly in pegmatites. It also occurs as an accessory mineral in black sands and other detrital deposits derived from gneissic or granitic terranes. It occurs associated with zircon, sphene, monazite, xenotime, allanite and various niobate-tantalates. Thorite color is mostly brown or brownish black (Fig. 22a) and represented by prismatic and cubic grains. Pure thorite grains were investigated under the Environmental Scanning Electronic Microscope (ESEM) as shown in figure 22b.

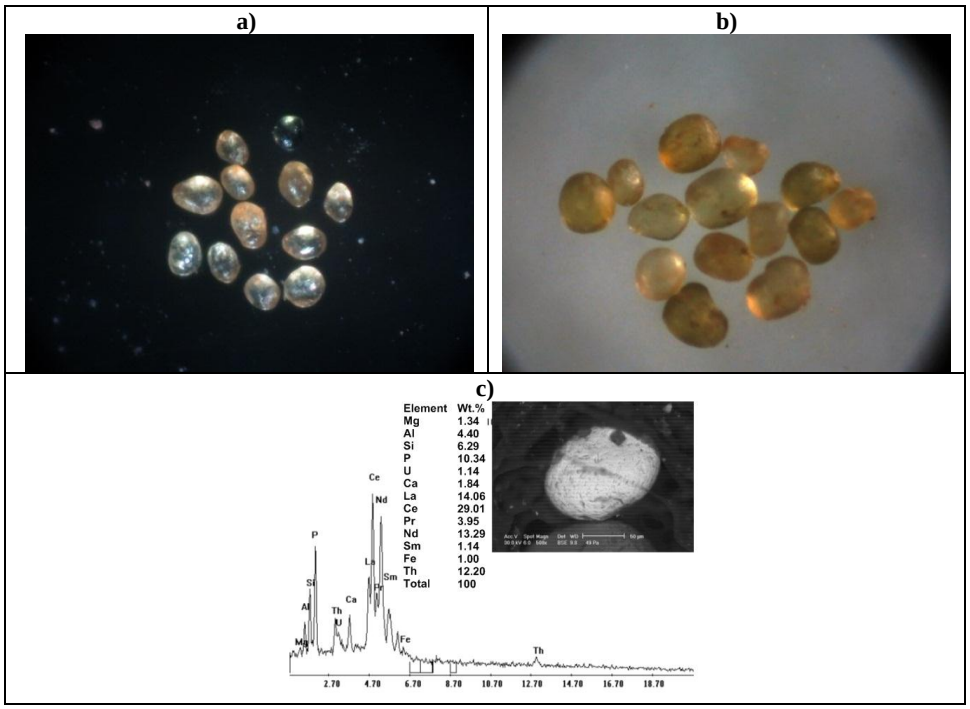


**Figure (18): Photomicrographs show:**

**a) Colorless rounded and oval shape of monazite grains, X25.**

**b) Lemon yellow rounded and oval shape of monazite grains, X25.**

**c) EDX and BSE image of pure monazite grain.**

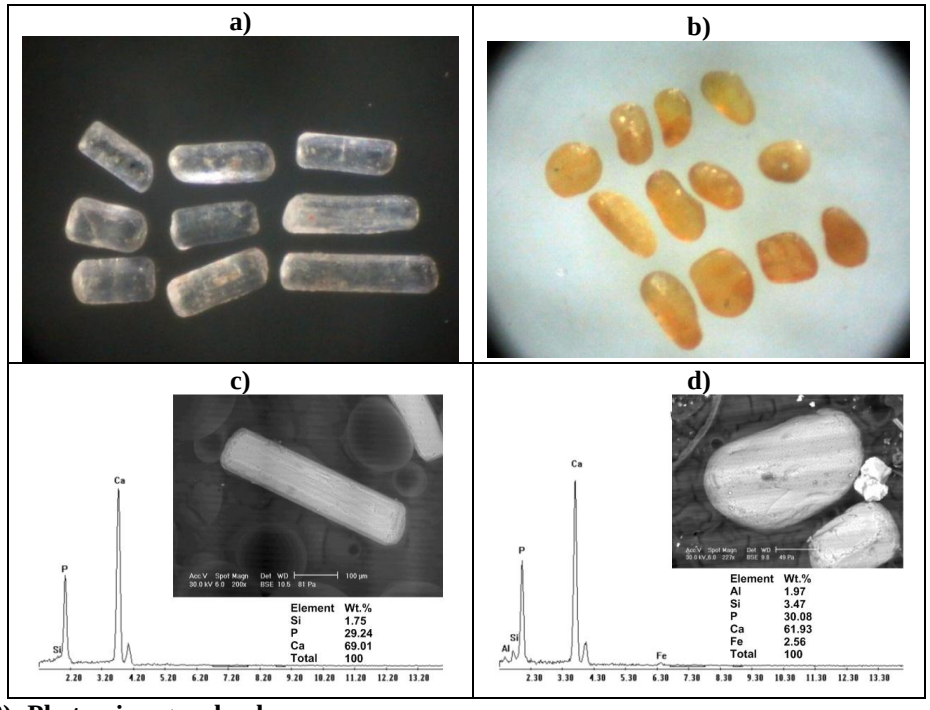


**Figure (19): Photomicrographs show:**

**a) Prismatic colorless apatite, X35.** **b) Yellow apatite, X25.**

**c) EDX and BSE image of pure colorless prismatic apatite grain.**

**d) EDX and BSE image of pure oval apatite grain.**

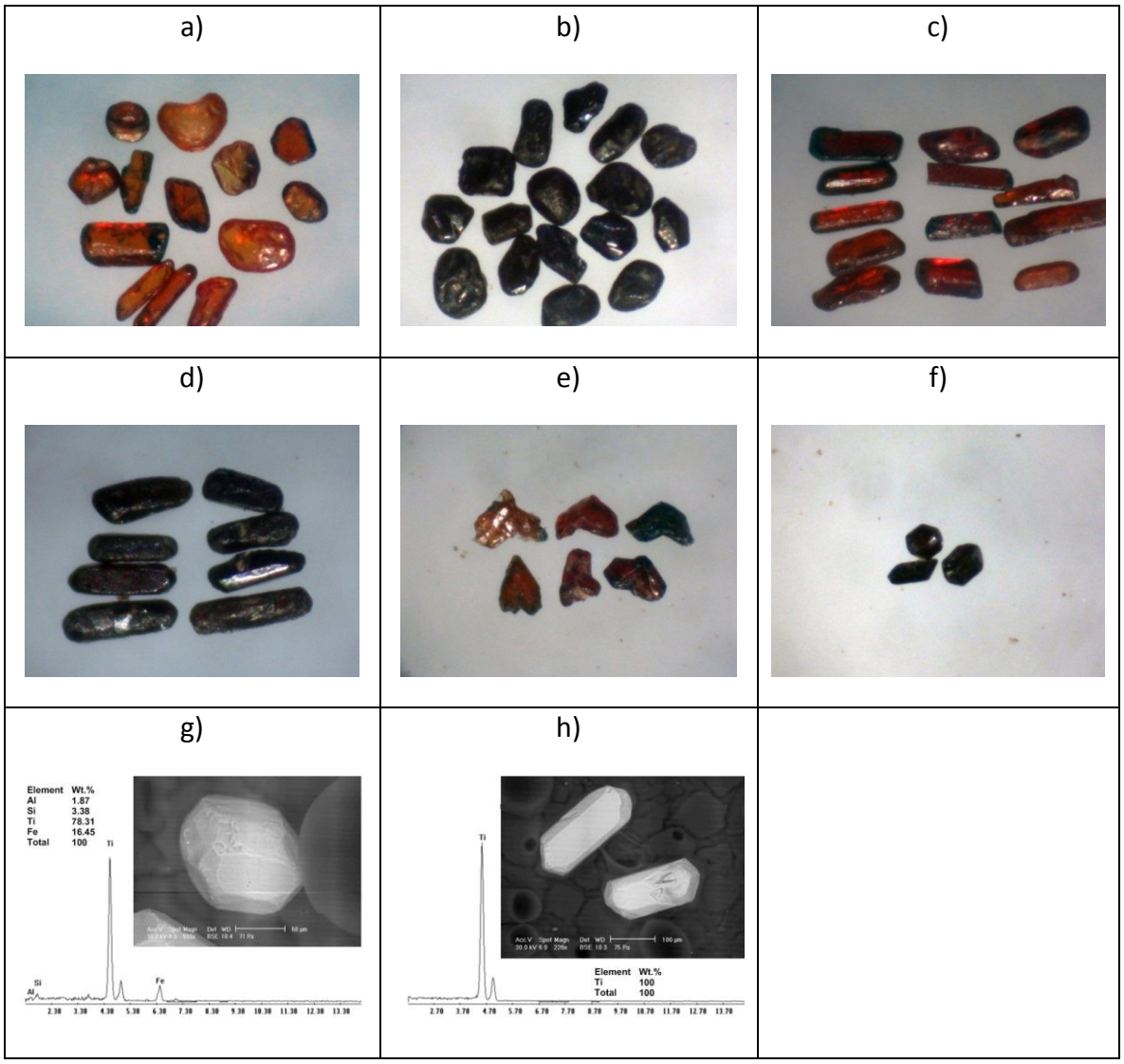


**Figure (20): Photomicrographs show:**

**a) Rounded red rutile grains, X35. b) Rounded black rutile grains, X35.**
**c) Prismatic red rutile grains, X35. d) Prismatic black rutile grains, X35.**
**e) Chevron (elbow) red rutile grains, X35. f) Euhedral ditetragonal dipyramidal black rutile crystals, X35.**
**g) EDX and BSE image of pure black rutile grain. h) EDX and BSE image of pure red rutile grain.**

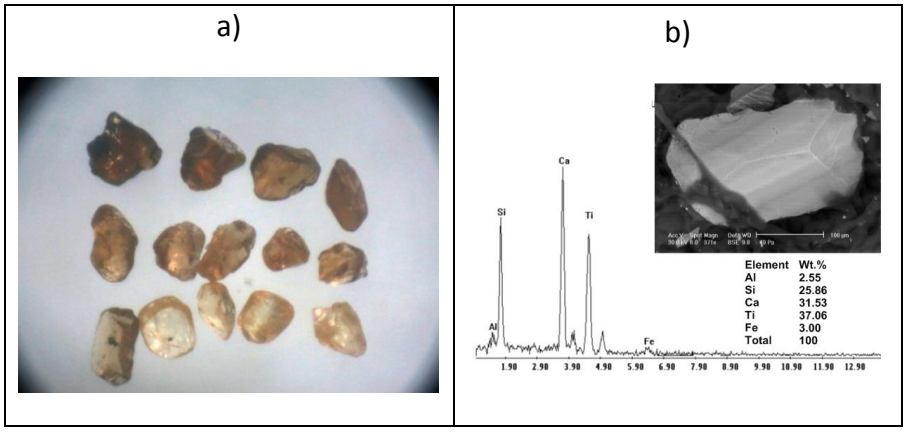


**Figure (21): Photomicrographs show:**

**a) Yellowish to brownish yellow titanite grains, X25. b) EDX and BSE image of pure titanite grain.**

**Radiometric**

The radioactivity of the studied sediments is mainly attributed to the presence of the three radioactive minerals, zircon, monazite and thorite. The uranium and thorium contents in the studied 64 samples has been collected from the studied area to determine variations in eU, eTh, Ra and K%. The obtained results from the radiometric measurements of the studied stream sediments are listed in table 6, the Min, Max. and Aveg. of these measurements are tabulated in table 7.

The examined sediments of studied area are characterized by radiometrically (low) concentrations of eU and eTh. The radiometrically elemental concentration of eU range between U/D and 4ppm with an average of 1.3ppm, while eTh is between 2 and 17ppm with an average of 5.61ppm. The average Ra content for these sediments is 1.66 ppm, ranging between 1and 4ppm. The average content of K% 0.61%, ranging between 0.68 and 1.25%.

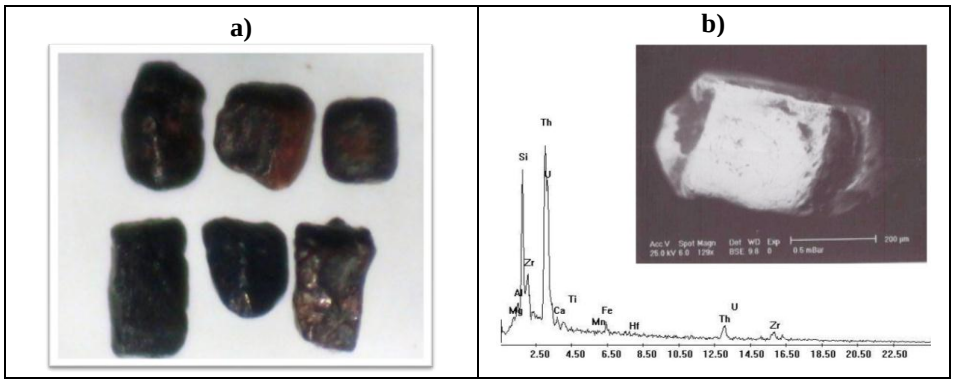


**Figure (22): Photomicrographs show:**
**a) Reddish black thorite grains, X25. b) EDX and BSE image of pure thorite grain.**

**Table (6): The distribution of radiometric measurements of the studied samples.**

| S. No. | eU ppm | eTh ppm | eRa ppm | K% | S. No. | eU ppm | eTh ppm | eRa ppm | K% | S. No. | eU ppm | eTh ppm | eRa ppm | K% | S. No. | eU ppm | eTh ppm | eRa ppm | K% |
|---|---|---|---|---|---|---|---|---|---|---|---|---|---|---|---|---|---|---|---|
| **1.1** | U/D | 17 | 4 | 1.25 | **5.4** | 1 | 4 | 1 | 0.82 | **8.2** | 2 | 6 | 2 | 0.41 | **12.1** | U/D | 2 | 1 | 0.37 |
| **1.2** | 1 | 13 | 3 | 0.78 | **5.5** | 2 | 6 | 2 | 0.73 | **8.3** | U/D | 7 | 3 | 0.35 | **12.2** | 1 | 3 | 2 | 0.35 |
| **2.1** | 1 | 11 | 3 | 0.66 | **5.6** | U/D | 3 | 1 | 0.64 | **8.4** | 0.8 | 5 | 2 | 0.37 | **12.3** | U/D | 5 | 1 | 0.31 |
| **2.2** | U/D | 14 | 2 | 0.56 | **5.7** | U/D | 5 | 1 | 0.56 | **9.1** | U/D | 3 | 3 | 0.76 | **12.4** | 1 | 4 | 1 | 0.40 |
| **2.3** | 1 | 14 | 3 | 0.52 | **5.8** | 1 | 4 | 1 | 0.85 | **9.2** | 1 | 4 | 2 | 0.70 | **12.5** | 2 | 3 | 1 | 0.39 |
| **2.4** | 1 | 12 | 2 | 0.75 | **6.1** | 1 | 4 | 2 | 0.80 | **9.3** | U/D | 2 | 3 | 0.68 | **13.1** | U/D | 6 | 1 | 0.35 |
| **2.5** | U/D | 9 | 1 | 0.45 | **6.2** | U/D | 7 | 2 | 0.75 | **9.4** | 1 | 8 | 2 | 0.64 | **13.2** | 2 | 4 | 1 | 0.32 |
| **2.6** | 1 | 6 | 2 | 0.62 | **6.3** | 1 | 6 | 3 | 0.86 | **9.5** | 1 | 6 | 2 | 0.59 | **13.3** | 2 | 3 | 1 | 0.30 |
| **3.1** | U/D | 3 | 1 | 0.79 | **6.4** | 1 | 4 | 2 | 0.76 | **10.1** | U/D | 3 | 1 | 0.57 | **14.1** | U/D | 2 | 1 | 0.32 |
| **3.2** | 1 | 4 | 1 | 0.63 | **6.5** | U/D | 8 | 2 | 0.68 | **10.2** | 1 | 5 | 1 | 0.56 | **14.2** | 1 | 4 | 2 | 0.30 |
| **4.1** | U/D | 7 | 2 | 1.03 | **6.6** | U/D | 5 | 2 | 0.57 | **10.3** | 1 | 4 | 2 | 0.60 | **14.3** | 1 | 2 | 1 | 0.29 |
| **4.2** | 2 | 5 | 1 | 0.84 | **6.7** | U/D | 6 | 1 | 0.72 | **10.4** | U/D | 6 | 2 | 0.51 | **14.4** | U/D | 3 | 1 | 0.28 |
| **4.3** | U/D | 3 | 1 | 0.68 | **6.8** | U/D | 5 | 1 | 0.67 | **10.5** | U/D | 3 | 1 | 0.49 | **15.1** | 1 | 5 | 2 | 0.75 |
| **5.1** | 2 | 4 | 2 | 1.02 | **7.1** | U/D | 8 | 2 | 0.60 | **11.1** | 2 | 5 | 1 | 0.43 | **15.2** | 1 | 4 | 1 | 0.71 |
| **5.2** | 1 | 3 | 2 | 0.94 | **7.2** | 1 | 7 | 1 | 0.63 | **11.2** | 1 | 7 | 1 | 0.50 | **15.3** | 1 | 2 | 1 | 0.72 |
| **5.3** | U/D | 5 | 1 | 0.76 | **8.1** | 4 | 10 | 3 | 0.38 | **11.3** | U/D | 6 | 1 | 0.43 | **15.4** | U/D | 5 | 1 | 0.68 |

**Table (7): The Min, Max. and Aveg. of the studied samples.**

| | eU ppm | eTh ppm | eRa ppm | K% |
|---|---|---|---|---|
| **Min** | U/D | 2 | 1 | 0.68 |
| **Max.** | 4 | 17 | 4 | 1.25 |
| **Aveg.** | 1.3 | 5.61 | 1.66 | 0.61 |

## CONCLUSION

Nasser Lack area is delineated by Latitudes 22°00′ –23°58′ N and Longitudes 30°07′–33°15′ E, covered by 64 samples. The identified heavy mineral assemblages can be classified into two main groups. The first one is the opaque minerals as; magnetite, hematite, ilmenite, leucoxene, vanadium, chromite, pyrite, atacamite, alumina minerals, gold and silver. The second group is non-opaque minerals includes garnet, monazite, rutile, zircon, titanite, apatite and green silicates.

The calculated percentages of these minerals are as follow. The first group is the opaque minerals as magnetite which ranging from 0.001%- 1.973% with an average of 0.253%, Hematite ranging from 0.005%-0.241% with an average of 0.048%, Ilmenite ranging from 0.026%-4.413% with an average of 0.616% and Leucoxene ranging from 0.014%-1.247% with an average of 0.316%. Native minerals include gold ranging from Nil - 0.107% with an average of 0.008% and silver ranging from Nil -0.058% with an average of 0.004%. The second group is non-opaque minerals include zircon ranging from 0.031%-4.151% with an average of 0.495%, garnet ranging from 0.004%-0.310% with an average of 0.045%. monazite ranging from 0.001%-0.089% with an average of 0.009%, apatite ranging from 0.001%- 0.262% with an average of 0.028%, rutile ranging from 0.015%-2.199% with an average of 0.399%, titanite ranging from 0.002%- 0.611% with an average of 0.065% and green silicates ranging from 0.008% – 14.049% with an average of 1.386%.

The examined sediments of studied area are characterized by radiometrically (low) concentrations of eU and eTh. The radiometrically elemental concentration of eU ranges between U/D and 4ppm with an average of 1.3ppm, while eTh is between 2 and 17ppm with an average of 5.61ppm. The average Ra content for these sediments is 1.66ppm, ranging between 1and 4ppm. The average content of K% 0.61%, ranging between 0.68 and 1.25%.

## REFERENCES

**Abul-Atta, A. A. (1978):** Egypt and Nile after the high dam. Cairo: Ministry of Irrigation and Land Reclamation.

**Armstrong, P., (1922)**: Zircon as ceriterian of igneous or sedimentary and metamorphic. Amer., Vol. 5(4), 395p.

**Carroll, D., (1953):** Weatherability of zircon . J. Sed. Pet., Vol. 23, 116p.

**Elewa H. (2006)** Water resources and geomorphological characteristics of Toshka and west of Lake Nasser, Egypt. Hydrogeol J 14 (6):942–954 (13) //Kim J, Sultan M (2002) Assessment of the long-term hydrologic impacts of Lake Nasser and related irrigation projects in Southwestern Egypt. J Hydrol 262(1–4):68–83.

**El-Kobtan, H. M. (2007):** Geological studies on the recent sediments of Lake Nasser (Southern Part) as a sign reflecting its evolution (MSc thesis). Benha University, Egypt.

**El-Kobtan, H., Salem, M., Attia, K., Ahmed, S. and Abou El-Magd, A., (2016):** Sedimentological study of Lake Nasser; Egypt, using integrated improved techniques of core sampling, X-ray diffraction and GIS platform. Cogent Geoscience (2016), 2: 1168069.

**Elsner. H., (2010)**: Heavy minerals of economic importance. Assessment manual, Faculty of Geosciences of the University of Hannover: 218p., 31 Fig. 125 Tab.

**El Ramly I. (1973):** Final report on geomorphology, hydrogeology, planning for groundwater resources and land reclamation in Lake Nasser Region and its environ. Reg. Plan. of Asw. Lake Nasser Cen. And Des. Inst. Cairo. A.R.E.

**Farhat, H. I. and Salem, S. G., (2015):** Effect of flooding on distribution and mode of transportation of Lake Nasser sediments, Egypt. Egyptian Journal of Aquatic Research (2015) 41, 165–176.

**Flinter, B. H., (1955):** A magnetic separation of some alluvial minerals in Malaya, Amer. Miner., Vol. 44, No. 7-8, 751p.

**Folk, R. L., (1980):** Petrology of sedimentary rocks. Univ. Texas, Hemphill, Pup. Co., Austin, Texas, USA.

**Gindy, N. N., (2015):** Environmental implications of electron microscope study of quartz grains' surface textures on khors sediments, Lake Nasser, Egypt. Egyptian Journal of Aquatic Research (2015) 41, 41–47.

**Goher , M. E., Farhat, H. I., Abdo, M. H. and Salem, S. G., (2014)** Metal pollution assessment in the surface sediment of Lake Nasser, Egypt. Egyptian Journal of Aquatic Research (2014) 40, 213–224.

**Groves, A. W., (1930):** The heavy minerals suite and the correlation f the granites of northern Brittany, The channel Islands and the cotentin, Geol. Mag., Vol. 67, 240p.

**Hammoud, N. S. and Khazback, A. E., (1984):** Traces of native gold particles in Egyptian northern beach heavy minerals deposits. Egypt: Jour. Geol. Vol. 28, p. 79-82.

**Hassaan, A. H. A., (2005):** Evaluation of the heavy minerals in the coastal sand dunes, East Sabkhit Al-Tinna, North Sinai, Egypt. Ph. D. thesis, Fac., of Sci., Ain Shams Univ.

**Hassaan, M. M. and ElDardir, M., (1987):** Sedimentation, grain size and mineral composition of the bottom sedimentsof the Aswan High Dam reservoir. Egypt: 6 th Symp. Quaternary and development in Egypt (abstracts), March, 1987, p. 11-12.

**Hassaan, M. M., ElDaedir, M. and Nassar, Y. Z., (1995):** Alluvial gold placer in main sedimentation area, High Dam Lake, Egypt: the first record. Sedimentology of Egypt, Vol. 3, p. 125-129.

**Khedr, E., Abou Elmagd, K. and Halfawy, M., (2014):** Rate and budget of blown sand movement along the western bank of Lake Nasser, southern Egypt. Arab J Geosci (2014) 7:3441–3453

**Kim, J. and Sultan, M., (2002):** Assessment of the long-term hydrologic impacts of Lake Nasser and related irrigation projects in Southwestern Egypt. J Hydrol 262(1–4):68–83

**Makary A. Z. (1982):** Sedimentation in the high aswan dam reservoir (PhD thesis). Ain Shams University, Cairo.

**Mohamed, E. H., (1987):** Mineralogical studies for some Quaternary sediments in northern Sinai. M. Sc. Thesis, IsmailiaUniv.

**Mohamed, S. S. M., (1998):** radioactivity and mineralogic studies on wadi Abu Dabbab alluvial deposits, Central Eastern Desert, Egypt. M. Sc. Thesis, Fac. of Sci., Ain Shams Univ. 204p.

**MÜcke, A. (2003):** Magnetite, ilmenite and ulvite in rocks and ore deposits: petrography, microprobe analyses and genetic implications.- Mineralogy and Petrology, 77: 215-234, 6 fig., 2 tab.; Vienna.

**Muller, G., (1967)**: Methods in sedimentary petrology. Sluttgart, E. Schweizerbartsche Verlagsbuchhandlung, 283p.

**Philip, G., Hassan, F., & Khalil, I. (1978):** Mechanical analysis and mineral composition of Lake Nasser (Lake Nasser and River Nile project, Report prepared to Academy Science Research and Technology). Egypt.

**Phillips, W. R. and Griffen, D. T., (1981):** Optical mineralogy, the non opaque minerals. Freeman and Company, Sanfrancisco. U.S.A.

**Poldervart, A., (1955):** Zircon in sedimentary rocks. Am. J. Sci., Vol. 433, 461p.

**Poldervart, A., (1956):** Zircon in igneous rocks. Am. J. Sci., Vol. 254, 554p.

**Said, R., (1981):** The geological evolution of the River Nile. Springer, New York, 151 pp.

**Saxena, S. K., (1966):** Evaluation of zircon in sedimentary and metamorphic rocks. J. Sed., Vol. 2, 33p.

**Shalash, S. (1980):** Effect of sedimentation on storage capacity of high aswan dam reservoir (Nile Research Institute Report, National water Research Center). Cairo.

**Springuel, I. V., Hassan, L. M., Sheded, M., El-Soghir, M., & Ali, M. M., (1991):** Plant ecology of Wadi Allaqi and Lake Nasser. 3. Flora of the Wadi Allaqi basin (Allaqi Project Working Paper No. 10). Glasgow: University of Glasgow.

**Surour, A. A., El Kammar, A. A., Arafa, E. H. and Korany, H. M., (2003)-** Dahab stream sediments, South Eastern Sinai, Egypt : a potential source of gold, magnetite and zircon. Journal of Geochemical Exploration Vol. 77 ( 2003 ), 43p.

**Ward, J. & Towner, R. (1985b)**: Japan.- in: UNESCAP & BMR: Mineral sands in Asia and the Pacific.- Mineral concentrations and hydrocarbon accumulations in the ESCAP region, 4: 76– 80, 1 fig., 4 tab.; w/o place, Australia.

# معدنية واشعاعية الجزء الجنوبي من رواسب بحيرة ناصر مصر

**اشرف العزب ، سامح الألفي و هاني حسن**

**هيئة المواد النووية – ص. ب. ٥٣٠ المعادي- القاهرة –مصر**

## الملخص العربي

تقع بحيرة ناصر بين خطى عرض ٢٢° ٠٠′و٢٣° ٥٨′ شمالا وخطى طول مابين ٣٠° ٠٧′ و٣٣° ١٥′ شرقا.وقد تم جمع ٦٤ عينة تغطى هذه المنطقه لدراسة المعادن الاقتصادية الثقيلة بهذه العينات حيث وجد ان المنطقة تحتوى على مجموعتين من المعادن:

١- معادن معتمة تتمثل في معادن الماجنتيت والهيماتيت والالمنيت واليكوكزين بالاضافه الى الفانديوم والكروم والبيريت والاتاكميت والالومنيوم والذهب والفضة.

٢- معادن شفافة وشبه شفافة وتتمثل في الجارنت والروتيل والمونازيت والزيرقون والتيتانيت والاباتيت بالاضافة الى معادن السليكا الخضراء.

وقد اتضح من خلال الدراسة ان هذه المنطقة ضعيفة اشعاعيا حيث يصل تركيز اليورانيوم ما بين منعدم الى ٤ جزء في المليون بمتوسط يصل الى ١,٣ جزء في المليون والثوريوم يتراوح ما بين ٢ الى ١٧ جزء في المليون بمتوسط يصل الى ٥,٦١ جزء في المليون والرادون يتراوح ما بين ١ الى ٤ جزء في المليون بمتوسط يصل الى ١,٦٦ جزء في المليون بينما البوتاسيوم يتراوح مابين ٠,٦٨ % الى ١,٢٥% بمتوسط يصل الى٠,٦١% مما يعني امكانية استغلال خامات هذه المنطقة اقتصاديا دون التأثير السلبي على البيئة.